




Tunable microcavities coupled to rare-earth quantum emitters

KANGWEI XIA,^{1,6,†} FIAMMETTA SARDI,^{1,7,†} COLIN SAUERZAPF,¹ THOMAS KORNHER,² HANS-WERNER BECKER,³ ZSOLT KIS,⁴ LASZLO KOVACS,⁴  DENIS DERTLI,¹ JONAS FOGLSZINGER,¹ ROMAN KOLESOV,¹ AND JÖRG WRACHTRUP^{1,5}

¹Physikalisches Institut, University of Stuttgart, 70569 Stuttgart, Germany

²Lumiphase AG, 8802 Kilchberg, Switzerland

³RUBION, Ruhr-Universität Bochum, 44780 Bochum, Germany

⁴Wigner Research Center for Physics, Institute for Solid State Physics and Optics, H-1121 Budapest, Hungary

⁵Max Planck Institute for Solid State Research, 70569 Stuttgart, Germany

⁶e-mail: kangwei.xia@pi3.uni-stuttgart.de

⁷e-mail: f.sardi@pi3.uni-stuttgart.de

Received 10 January 2022; revised 24 February 2022; accepted 7 March 2022; published 14 April 2022

Electro-optical control of on-chip photonic devices is an essential tool for efficient integrated photonics. Lithium niobate on insulator (LNOI) is an emerging platform for on-chip photonics due to its large electro-optic coefficient and high nonlinearity. Integrating quantum emitters into LNOI would extend their versatility in classic photonics to quantum computing and communication. Here, we incorporate rare-earth ion (REI) quantum emitters into electro-optical tunable lithium niobate (LN) thin films and demonstrate control of LN microcavities coupled to REIs over a frequency range of 160 GHz with 5 μ s switching speed. Dynamic control of the cavities enables modulation of the Purcell enhancement of REIs with short time constants. Using Purcell enhancement, we show evidence of detecting single Yb^{3+} ions in LN cavities. Coupling quantum emitters in fast tunable photonic devices is an efficient method to shape the waveform of the emitter. It also offers a platform to encode quantum information in the integration of a spectral–temporal–spatial domain to achieve high levels of channel multiplexing, as well as an approach to generate deterministic single-photon sources. © 2022 Optica Publishing Group under the terms of the [Optica Open Access Publishing Agreement](#)

<https://doi.org/10.1364/OPTICA.453527>

1. INTRODUCTION

Solid-state spin qubits, such as quantum dots and defects in solids, are promising candidates for realizing quantum networks with applications ranging from quantum computing and communications to quantum sensing due to their long spin coherence and the ability of optical interfacing [1–3]. Among different types of optically addressable spin qubits, rare-earth ions (REIs) in solids have recently emerged as promising systems. They offer advantages in both optical and spin aspects: various emission wavelengths including telecom band compatible with fiber quantum networks and spin transitions with long coherence times enabling long-lasting quantum memory [4–9]. However, the $4f-4f$ dipole forbidden optical transitions of REIs make optical readout at the single-ion level challenging [10,11]. Incorporation of REIs into photonic cavities is an efficient approach to enhance the quantum light–matter interface, where the lifetime of REIs reduces due to the Purcell effect [12–16]. This leads to the enhancement of emission at single-ion levels [17,18]. Coupling of REIs to cavities results in the recent demonstrations of nondemolition measurement of single REI qubits and multi-qubit readout within a single diffraction-limited volume [19–21].

Quantum hardware based on single REIs allows for fully scalable architecture [22]. To achieve the scalability, one has to equip each REI with its own resonator. There are two key ingredients in this approach: (1) individual tunability of RE emitters to bring them to the same optical frequency so that the photons emitted by them can interfere and (2) individual tunability of their Purcell enhancement to control their interaction with the environment, i.e., tunability of the cavity the emitter is in. Furthermore, Purcell enhancement control should be fast, much faster than the lifetime of the excited state of REIs. With these ingredients, one gains full control over ion-cavity qubits. If realized, this approach would result in practically unlimited scalable hardware for linear quantum computing. The tunability of emitters can be achieved by the Zeeman effect or Stark shift [23]. In this work, we address the second ingredient, namely, dynamic control of Purcell enhancement.

Directly modifying the refractive index of electro-optical materials via an external electric field is a straightforward method to individually tune the frequencies of the cavities. It results in a large frequency tuning range, fast controlling speed, and more importantly, the ability of independent control of the integrated cavities. Lithium niobate (LN) is a key optical material [24] due

to its large electro-optic coefficients [25], broad transmission window, and nonlinearity [26], with various applications, such as electro-optical modulators [27], coherent photon conversion, and quantum memories [28,29]. The recent commercialization of LN on insulator (LNOI) offers an attractive platform to highly integrate photonic devices on-chip [30,31]. The low operation voltage and fast electro-optical modulation speed results in a variety of attractive applications, ranging from broadband frequency comb generation [32] and fast electro-optic modulators [27,33] to high-quality factor cavities [34], micro-lasers [35], and more [36]. However, LNOI has not shown similar functionality in integrated quantum technology. A direct quantum functionalization with quantum emitters has not yet been achieved. Here, we directly dope REIs in LN thin films by means of ion implantation [37]. We perform hole-burning spectroscopy (HBS) of Yb-implanted LNOI and show that post-annealing at 650°C is sufficient to achieve spectrally narrow excitation of Yb³⁺ ions, as well as excellent charge stability. This procedure is also compatible with fabricating photonic elements, such as electro-optically tunable high-*Q* microcavities. With these elements, we are able to modulate the Purcell effect of Yb³⁺ ions dynamically. By coupling REIs to the cavity and hence increasing their emission rate, we provide evidence of detecting single Yb³⁺ ions.

2. DEVICE DESIGN AND CHARACTERIZATION

In experiments, we implant Yb ions with an energy of 1.5 MeV and a fluence of 10¹² ions/cm² into LN films. According to the stopping and range of ions in matter (SRIM) simulation, the implanted ions are located at 261 nm depth with 71 nm spatial distribution in the *z* axis (see Fig. S4 in Supplement 1). After ion implantation, we further post-anneal the Yb-implanted LN thin film at 650°C in air without observing any damage to the film. The annealing temperature is still 500°C lower than required for Yb doping of LN during crystal growth. Thus, before using the REI-implanted thin film, further characterization is needed to evaluate their optical properties. We perform HBS [38] to assess the quality of the implanted Yb ions in the LN waveguide and Yb-doped bulk LN crystal at cryogenic temperatures (3.5 K) (experimental details are described in Supplement 1 Note 4). The Yb-doped bulk crystal is a congruent crystal with 6% Mg doping, and it was grown by the Czochralski method with a concentration of 0.01% of Yb [39]. Yb-doped LN bulk crystal shows spectral hole widths of 2π × 58 MHz, while the Yb-implanted LN long waveguide shows 2π × 82 MHz. The results suggest that post-annealing at 650°C is sufficient to activate and stabilize the implanted Yb ions in LN thin films, showing a similar optical performance to the one in a bulk crystal. This gives us a simple approach to directly incorporate REIs in pre-fabricated photonic devices, based on commercially available LN thin film. The broad spectral hole width of Yb:LN is mainly due to the nuclear spin bath. The exploitation of isotopes having clock transitions will be an invulnerable method to suppress fluctuations of the spin bath of LN [40,41].

We further shape the Yb-implanted LN thin film to microcavities (the fabrication protocol is described in Supplement 1 Note 3). A scanning electron microscope (SEM) image of one of the cavities is shown in Fig. 1(b). The microdisk resonator has a size of 7 μm radius. A waveguide positioned next to the microdisk evanescently couples light into and out of the cavity. To enhance its output efficiency, a 45° undercut is milled at the ends of the waveguide. The typical *Q*-factor of the fabricated cavities is in the

range of 50,000–150,000 with a mode volume $V_{\text{mode}} = 50(\frac{\lambda}{n})^3$. The highest *Q*-factor of the cavity is 244,730, as shown in Fig. 1(c). The spectrum shows a doublet mode (split mode). The whispering gallery mode resonator has two degenerate modes with the same resonant frequency and field distributions and opposite propagation directions, which are clockwise and counterclockwise modes. This degeneracy is lifted and splits the resonance into a doublet if the resonator deviates from its perfect azimuthal symmetry due to any perturbation in the mode volume, such as surface roughness, material inhomogeneity, or a scattering point because of the presence of nanoparticles and defects along the sidewalls of the microdisk resonator [42]. According to simulations, the *Q*-factor of the microdisk can exceed 10⁹ when only radiative loss is considered. The *Q*-factor of the current cavities is mainly limited by scattering losses that can be further improved by optimizing the fabrication protocol.

To achieve electro-optic tunability, an additional layer of indium tin oxide (ITO) is deposited on the LN cavity serving as the top electrode, with a 1 μm thickness negative photoresist (SU-8) serving as a spacer. The Si substrate acts as the bottom electrode [see Fig. 1(a)]. By applying a bias voltage between the electrodes, the reflective index of the LN cavity is modulated, resulting in the tuning of the cavity resonance frequency, as shown in Fig. 1(d). We further estimate the device's electro-optic coupling by applying ±60 V external voltage with a step width of 15 V. The response of the cavity turns out to be linear, indicating the absence of hysteresis from our device, with a coefficient of 270 MHz/V. In the experiment, a maximum voltage of ±300 V is applied, corresponding to the tuning range of ±81 GHz.

3. YB:LNOI TUNABLE MICROCAVITIES

With electro-optical tuning, the cavity frequency can be brought in and out of resonance with Yb³⁺:LN. For cavity quantum electrodynamics (QED) experiments, a microdisk with a *Q*-factor of 79,833 and high coupling between the cavity and the waveguide is further investigated. To achieve high detection efficiency, resonant excitation and resonant detection of Yb:LN is applied by placing a chopper in front of the detector. The scheme of the experimental setup is drawn and introduced in Supplement 1 (Fig. S3 and Note 1.3). The chopper blocks and opens the detector while the excitation laser is on and off. This results in pulsed-like lifetime measurement data. The rising slope of the chopper is ~2 μs, much longer than the laser energy dissipation time in the cavity (~100 ps).

Experimentally, when the frequency of the cavity is tuned on resonance with the zero phonon line of Yb:LN, we observe a shortening of the Yb³⁺ lifetime in the cavity, as shown in Fig. 2(a). The experiment is performed at cryogenic temperature (8 K). A cumulative distribution function is applied to fit the decay curve, resulting in 38 μs lifetime. The different shortening of the lifetime suggests that Yb³⁺ ions couple to the cavity with different strengths because of their different positions in the cavity. The lifetime in bulk Yb:LN is 430 ± 2 μs. Hence, Yb³⁺ coupling to the cavity results in a Purcell factor of 10.24. The lifetime shortening is three times lower than the theoretical estimation based on *Q*/*V* ratio. This is presumably caused by implanted Yb ions, which are spatially not located at the maximum of the cavity mode electric field.

In the following, fast electro-optic dynamic control of the microcavity coupled to REIs is demonstrated. (1) The frequency

of the cavity is tuned on resonance with the Yb ions. (2) A laser pulse is generated to resonantly pump the Yb ions to excited states. (3) The excited Yb ions start to decay back to their ground state with $38.0 \mu\text{s}$ lifetime due to the cavity QED. (4) Before the Yb ions completely decay to the ground state, the cavity resonance frequency is tuned off resonance (54 GHz frequency detuning) from the excited Yb ions, thus prolonging their lifetimes from $38 \mu\text{s}$ to $430 \mu\text{s}$. Since this emission from Yb ions coupled to the cavity is now off resonance, the excitation is stored in the cavity and is not coupled to the waveguide (5). After a certain waiting time, the cavity is tuned back on resonance with the excited Yb ions, resulting in the restoration of fast decay of the Yb ions. The experiment was carried out with different waiting times, as shown in Fig. 2(b).

To determine the electro-optical switching time of the microcavity, measurements with fast time resolution are performed [see Fig. 2(c)]. According to the rising and falling slopes of the fluorescence signals, the switching time of the microcavity is $\sim 5 \mu\text{s}$, limited by the bandwidth of the high-voltage operational amplifier in use.

We further investigated the detection of a single ion, based on the increased fluorescence signal due to Purcell enhancement. In the experiment, a cavity with a Q-factor of 64,065 is used. Instead of at the center of the inhomogeneous line of Yb^{3+} , the cavity resonance frequency is tuned along the tail of the inhomogeneous line of 980 nm Yb^{3+} optical transition [more than 140 GHz away from the center of the inhomogeneous line, as shown in Fig. 3(a)]. A laser power of 22 nW is applied to excite single Yb ions. The respective photoluminescence excitation (PLE) spectrum is shown in Fig. 3(b), where discrete lines are observed. In total, 24 discrete lines are fitted with an average linewidth of $2\pi \times 247 \pm 9 \text{ MHz}$ (Supplement 1 Note 5). We further plot one of the peaks, as shown in Fig. 4, with a fitted linewidth of $2\pi \times 215 \pm 22 \text{ MHz}$. The linewidth is twice as large as the spectral hole width that we obtained by HBS of Yb^{3+} implanted in a LN waveguide [see Fig. 4(a)]. We suspect that the broadening is caused by spectral diffusion.

Another important feature of emitters coupled to cavities is their spectral stability. Often, the fabrication of optical cavities results in spectrally unstable emitters. We investigate the spectral

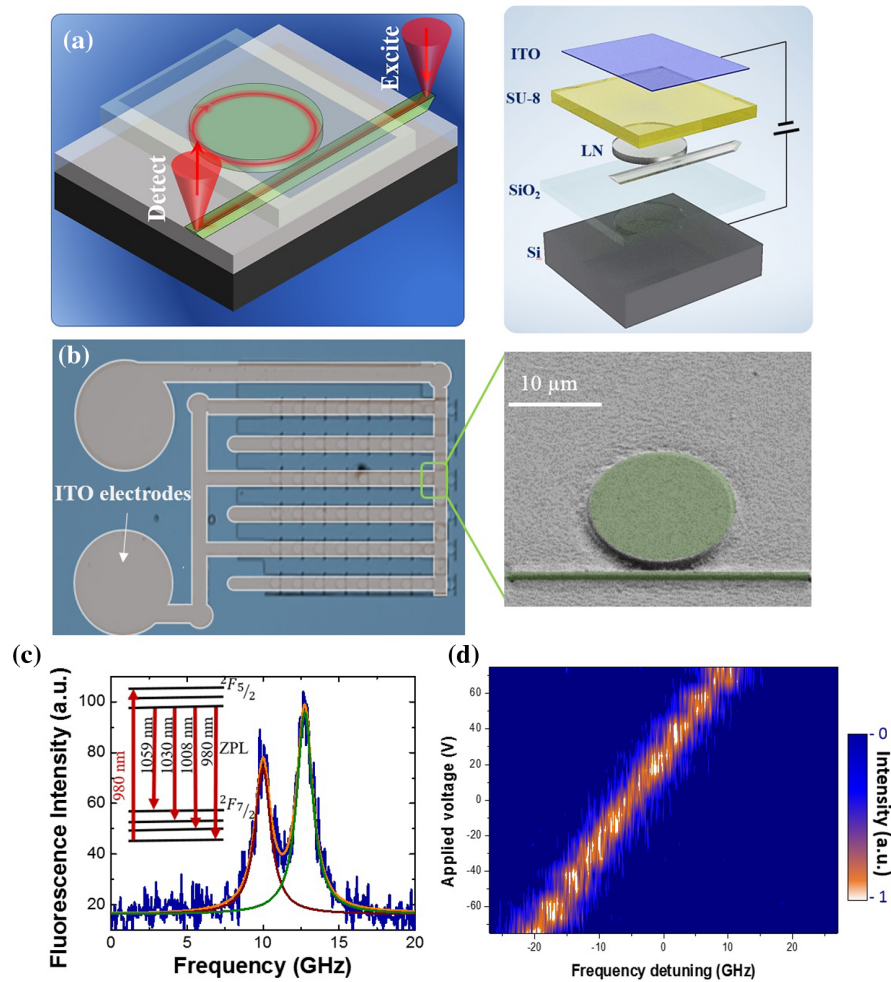


Fig. 1. Optical and electro-optical characterization of LN microdisks. (a) Schematics of our device. On a layer of amorphous SiO_2 , a microdisk with a waveguide is fabricated by e-beam lithography and etching. Photonic structures are capped with a layer of SU-8 on which we deposited a 30 nm layer of ITO. The right graph is an exploded view of the device design. (b) Optical images of fabricated microdisks on LN thin film with top ITO electrodes. The right graph is a SEM image of the microdisk. Incarnadine represents the ITO electrodes, and the green pattern shows the LN microdisk with coupling waveguide. (c) Linewidth of one of the monolithic LN microdisks fabricated on-chip with a Q-factor of 244, where the doublet is formed by the presence of nanoparticles and defects along sidewalls and surface of the microdisk. Inset shows the energy level of Yb:LN. (d) Electro-optic tuning of cavity mode depending on the bias voltage applied to the device with a coefficient of 270 MHz/V.

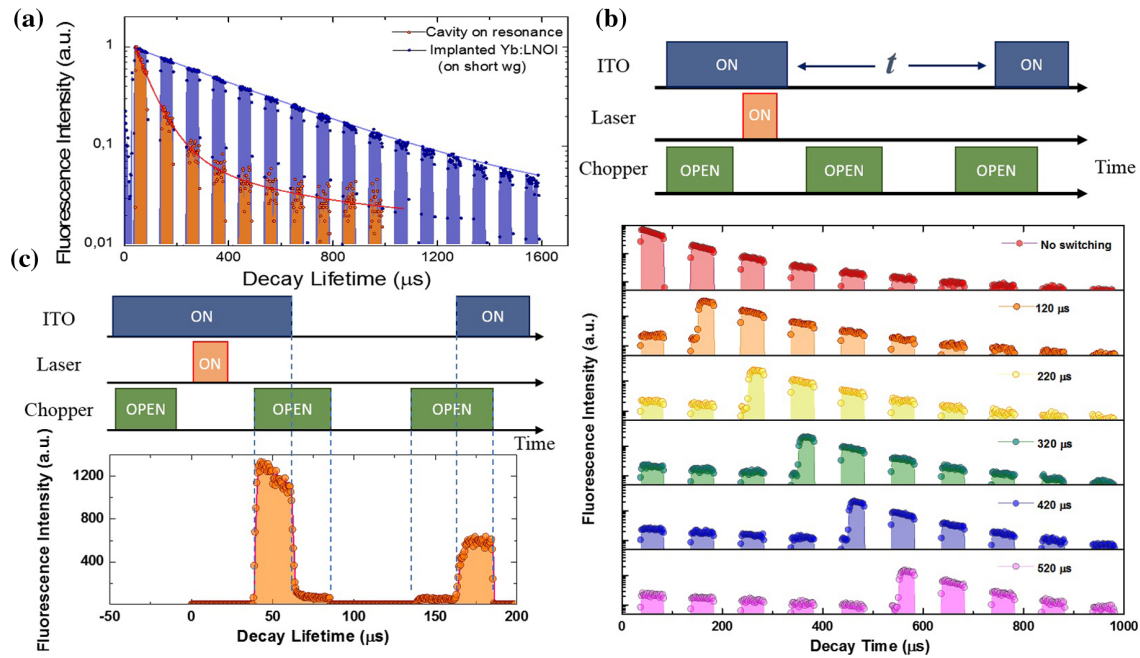


Fig. 2. Yb^{3+} in the LN microcavity. (a) Lifetime of implanted Yb ions in and out of resonance with the cavity. The blue curve shows a long decay time of $430 \mu\text{s}$ for off-resonance ions, and the red curve shows a shortened on-resonance decay lifetime. (b) Schematics of the fast-tuning protocol, showing how the cavity stores energy, when not on resonance with Yb ions. (c) High-resolution measurements to show the time constant of our device for frequency tuning. Switching is shown to occur of the order of $5 \mu\text{s}$, mainly limited by electronics.

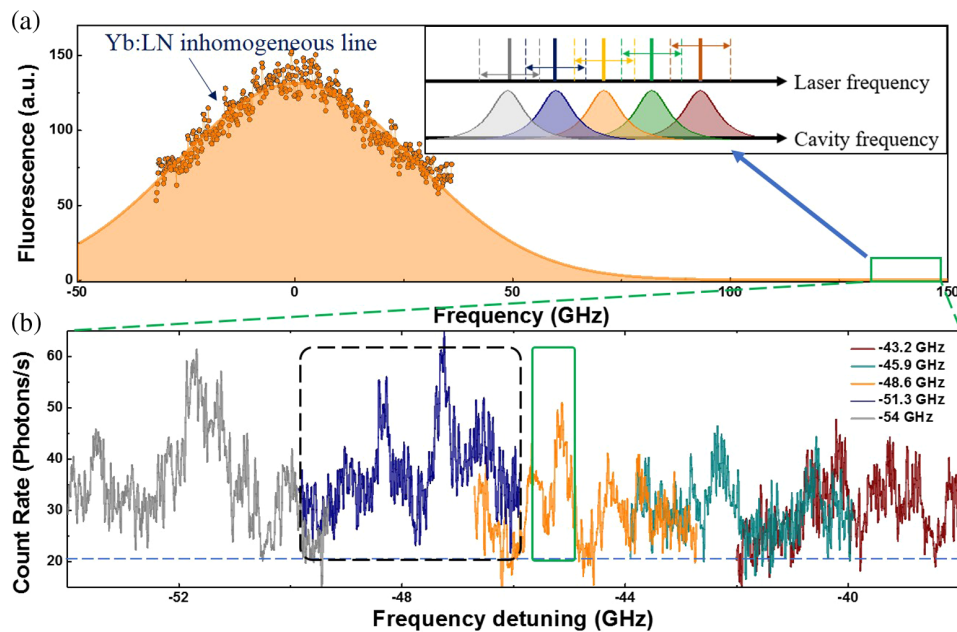


Fig. 3. Evidence of detecting single Yb ions in LN. (a) Inhomogeneous line of implanted Yb^{3+} in LN with a linewidth of $2\pi \times 64 \pm 0.6 \text{ GHz}$. The red and blue peaks indicate the frequency range in which the cavity can be tuned. The green rectangle marks the position where the PLE spectra of (b) are taken. The inset graph is a schematic of the experimental protocol. The frequency of the cavity is fixed to a certain position. The laser frequency is swept around the resonance frequency of the cavity. (b) PLE spectrum recorded at the tail of the inhomogeneous line profile of Yb implanted in LN marked. A cavity with a Q-factor of 64,065 is optically tuned from the center of the spectrum to the tail with a step width of 2.7 GHz and a total tuning range of 10 GHz . The discrete peaks have an average linewidth of $2\pi \times 247 \pm 10 \text{ MHz}$. Overlapping of peaks shows that the cavity can be electro-optically tuned back and forth across the spectrum.

stability by observing consecutive PLE measurements over an extended period of time [Fig. 4(d)]. Remarkably, we do not observe strong spectral diffusion. However, owing to a low count rate and 1:1 signal-to-background ratio of the Yb ions, it is challenging

to further analyze the spectral stability. In the future, with the improvement of the cavity Q-factor or smaller mode volume, the fluorescence signal will be enhanced, resulting in qualitative assessment of spectral stability.

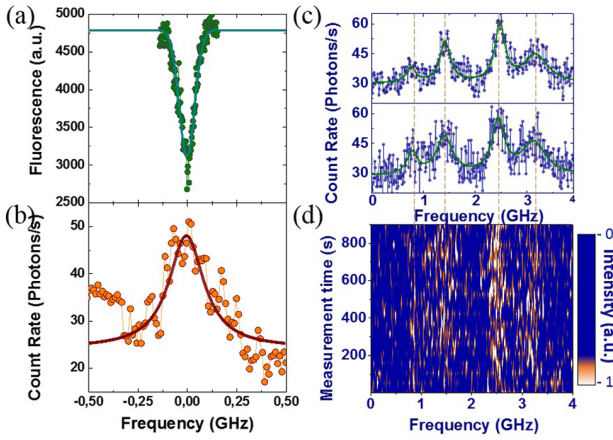


Fig. 4. Spectroscopy of single Yb ions in LN. (a) Hole burning spectroscopy of Yb implanted LN waveguide with a spectral hole width of $2\pi \times 97 \pm 2.3$ MHz. The experiment is performed at 8 K. (b) Plot of an individual PLE peak marked as a rectangle with green solid lines in Fig. 3(b). The linewidth is $2\pi \times 215 \pm 22$ MHz. (c) Single PLE spectrum of a sweep marked as a rectangle with black dashed lines in Fig. 3(a). The sweep is from lower frequency to higher frequency (upper curve) and reverse (lower curve). Both spectra show identical features, demonstrating that discrete peaks are not experimental artifacts but reproducible spectral features. (d) Acquisition of PLE spectra for more than 800 s over the same range as (c) showing no obvious spectral diffusion of ions inside the cavity.

Due to the flexible electro-optical tunability, we can detune the cavity resonance frequency in steps of 2.7 GHz and obtain PLE spectra in different ranges, as shown in Fig. 3(b). The total sweeping range is ~ 10 GHz, which is two times broader than the intrinsic linewidth of the cavity.

According to the Purcell enhanced lifetime we measured, the count rate of single Yb^{3+} in a LN cavity is calculated to be 9000 photon/s. The total amount of detected photons is estimated to be

$$9000 \times \eta_c(30\%) \times \eta_o(30\%) \times \eta_e(50\%) \times \eta_m(70\%) \\ \times \eta_{\text{chopper}}(50\%) \times \eta_d(60\%) = 40 \text{ counts/s,}$$

where η_c is the coupling efficiency between the microcavity to the waveguide; η_o represents the output efficiency at the end of the waveguide; η_e indicates the signal collected from only one end of the waveguide; η_m is the collection and transmission efficiency of the optical microscopy; η_{chopper} is the duty cycle of the chopper; and η_d is the efficiency of the superconducting single-photon detector.

For the cavity studied in Fig. 2 (Fig. 3), the linewidth is 3.83 GHz (4.9 GHz); the Q-factor is 79,833 (64,065); and REI lifetime reduction is measured to be 38.0 μs (62.7 μs). The Purcell factor is $C = \Gamma_0/\Gamma_c - 1 = 10.3$ (5.9), where Γ_c , Γ_0 represent the decay rates of Yb:LNOI coupled to the cavity and the natural lifetime of the bulk Yb:LN, respectively. These measurements further allow us to estimate the QED parameters for our cavities as $(g, \kappa, \Gamma_0) = 2\pi \times (1.9 \text{ MHz}, 3.83 \text{ GHz}, 370 \text{ Hz})$ and $(2\pi \times (1.62 \text{ MHz}, 4.9 \text{ GHz}, 370 \text{ Hz}))$, where g , κ are related to the single-photon Rabi frequency and cavity decay rate, respectively. We further estimated that for two cavities, 91.1% (85.6%) of the Yb:LNOI fluorescence is emitted into the cavity mode, and the branching ratio (Debye-Waller factor) of emission into 980 nm transition is improved from 25% to 93.3% (89.1%).

Our PLE measurements show a count rate of discrete peaks of 20–30 counts/s, which is consistent with our estimation. According to single-molecule-spectroscopy [43] the discrete peaks [44,45] correspond to single Yb ions in the LNOI microcavity. Due to the low count rate and low signal-to-background ratio, we are not able to perform second-order correlation measurements to unambiguously support our assumption. Further improving the quality of the cavity will increase the Purcell factor and signal-to-background ratio. It will help to further measure the second-order correlation function and investigate the photostability of single Yb ions.

4. CONCLUSION

In conclusion, we incorporate REI quantum emitters into LN thin film with optical properties similar to native REIs. The electro-optic control of LN microcavities enables couplings of REIs to be controlled at 5 μs switching speed and over a 160 GHz frequency range. Facilitated by Purcell enhancement, we further observe single Yb^{3+} ions in the cavities. The demonstration of dynamic control of on-chip photonic devices enables the shaping of a single-photon waveform. The spectral, temporal, and spatial selections of the single ions coupled to cavities will be a flexible and scalable approach to encode quantum information by employing high levels of channel multiplexing. Controlling the cavities in and out of the resonance of single ions is a highly desirable method to generate deterministic single-photon sources. Incorporating other REI species such as Er^{3+} ions into LNOI will result in kHz optical linewidth and wavelength in the telecom band. It is a promising candidate for long distance quantum networks [46]. Furthermore, LN thin films and an additional spin-free material, such as a yttrium orthosilicate (YSO) thin film, can form a hybrid quantum system. Long-lived quantum memory can be dynamically controlled by the electro-optical tuning of LN photonic devices, which enables spectral multiplexing of quantum memories.

Funding. Deutsche Forschungsgemeinschaft (KO4999/3-1, GRK 2642, FOR 2724); FET-Flagship Project SQUARE; European Commission, EU via SMEL; European Commission, EU via Quantum Internet Alliance; Bundesministerium für Bildung und Forschung; Development and Innovation Fund of Hungary within the Quantum Technology National Excellence Program (Project Nr. 2017-1.2.1-NKP-2017-00001).

Acknowledgment. We thank Arkadiy Kolesov and Frank Thiele for their support with the experiment, and Dr. Matthias Widmann for helping with artwork design. We acknowledge the fruitful discussion with Dr. Qi-Chao Sun, Prof. Kai-Mei Fu, and Dr. Philippe Goldner. We thank Sabrina Jenne and Matthew Joliffe for language corrections.

Disclosures. The authors declare no conflicts of interest.

Data availability. Data underlying the results presented in this paper are available in Supplement 1.

Supplemental document. See Supplement 1 for supporting content.

[†]These authors contributed equally to this work.

REFERENCES

- W. Gao, A. Imamoglu, H. Bernien, and R. Hanson, "Coherent manipulation, measurement and entanglement of individual solid-state spins using optical fields," *Nat. Photonics* **9**, 363–373 (2015).
- M. Atatüre, D. Englund, N. Vamivakas, S. Lee, and J. Wrachtrup, "Material platforms for spin-based photonic quantum technologies," *Nat. Rev. Mater.* **3**, 38–51 (2018).

3. D. Awschalom, R. Hanson, J. Wrachtrup, and B. Zhou, "Quantum technologies with optically interfaced solid-state spins," *Nat. Photonics* **12**, 516–527 (2018).
4. F. Bussières, C. Clausen, A. Tiranov, B. Kozh, V. Verma, S. Nam, F. Marsili, A. Ferrier, P. Goldner, H. Herrmann, C. Silberhorn, W. Sohler, M. Afzelius, and N. Gisin, "Quantum teleportation from a telecom-wavelength photon to a solid-state quantum memory," *Nat. Photonics* **8**, 775–778 (2014).
5. M. Zhong, M. Hedges, R. Ahlefeldt, J. Bartholomew, S. Beavan, S. Wittig, J. Longdell, and M. Sellars, "Optically addressable nuclear spins in a solid with a six-hour coherence time," *Nature* **517**, 177–180 (2015).
6. E. Saglamyurek, J. Jin, V. Verma, M. Shaw, F. Marsili, S. Nam, D. Oblak, and W. Tittel, "Quantum storage of entangled telecom-wavelength photons in an erbium-doped optical fibre," *Nat. Photonics* **9**, 83–87 (2015).
7. Y. Ma, Y. Ma, Z. Zhou, C. Li, and G. Guo, "One-hour coherent optical storage in an atomic frequency comb memory," *Nat. Commun.* **12**, 2481 (2021).
8. X. Liu, J. Hu, Z. Li, X. Li, P. Li, P. Liang, Z. Zhou, C. Li, and G. Guo, "Heralded entanglement distribution between two absorptive quantum memories," *Nature* **594**, 41–45 (2021).
9. D. Lago-Rivera, S. Grandi, J. Rakonjac, A. Seri, and H. de Riedmatten, "Telecom-heralded entanglement between multimode solid-state quantum memories," *Nature* **594**, 37–40 (2021).
10. R. Kolesov, K. Xia, R. Reuter, R. Stöhr, A. Zappe, J. Meijer, P. Hemmer, and J. Wrachtrup, "Optical detection of a single rare-earth ion in a crystal," *Nat. Commun.* **3**, 1029 (2012).
11. P. Siyushev, K. Xia, R. Reuter, M. Jamal, N. Zhao, N. Yang, C. Duan, N. Kukharchyk, A. Wieck, R. Kolesov, and J. Wrachtrup, "Coherent properties of single rare-earth spin qubits," *Nat. Commun.* **5**, 3895 (2014).
12. D. Ding, L. Pereira, J. Bauters, M. Heck, G. Welker, A. Vantomme, J. Bowers, M. Dood, and D. Bouwmeester, "Multidimensional Purcell effect in an ytterbium-doped ring resonator," *Nat. Photonics* **10**, 385–388 (2016).
13. B. Casabone, J. Benedikter, T. Hümmer, F. Oehl, K. Lima, T. Hänsch, A. Ferrier, P. Goldner, H. de Riedmatten, and D. Hunger, "Cavity-enhanced spectroscopy of a few-ion ensemble in $\text{Eu}^{3+}:\text{Y}_2\text{O}_3$," *New J. Phys.* **20**, 095006 (2018).
14. B. Merkel, A. Ulanowski, and A. Reiserer, "Coherent and Purcell-enhanced emission from erbium dopants in a cryogenic high-resonator," *Phys. Rev. X* **10**, 041025 (2020).
15. B. Casabone, C. Deshmukh, S. Liu, D. Serrano, A. Ferrier, T. Hümmer, P. Goldner, D. Hunger, and H. de Riedmatten, "Dynamic control of Purcell enhanced emission of erbium ions in nanoparticles," *Nat. Commun.* **12**, 3570 (2021).
16. L. Weiss, A. Gritsch, B. Merkel, and A. Reiserer, "Erbium dopants in nanophotonic silicon waveguides," *Optica* **8**, 40–41 (2021).
17. A. Dibos, M. Raha, C. Phenicie, and J. Thompson, "Atomic source of single photons in the telecom band," *Phys. Rev. Lett.* **120**, 243601 (2018).
18. T. Zhong, J. Kindem, J. Bartholomew, J. Rochman, I. Craiciu, V. Verma, S. Nam, F. Marsili, M. Shaw, A. Beyer, and A. Faraon, "Optically addressing single rare-earth ions in a nanophotonic cavity," *Phys. Rev. Lett.* **121**, 183603 (2018).
19. M. Raha, S. Chen, C. Phenicie, S. Ourari, A. Dibos, and J. Thompson, "Optical quantum nondemolition measurement of a single rare earth ion qubit," *Nat. Commun.* **11**, 1605 (2020).
20. J. Kindem, A. Ruskuc, J. Bartholomew, J. Rochman, Y. Huan, and A. Haraon, "Control and single-shot readout of an ion embedded in a nanophotonic cavity," *Nature* **580**, 201–204 (2020).
21. S. Chen, M. Raha, C. Phenicie, S. Ourari, and J. Thompson, "Parallel single-shot measurement and coherent control of solid-state spins below the diffraction limit," *Science* **370**, 592–595 (2021).
22. A. Kinos, D. Hunger, R. Kolesov, K. Mølmer, H. de Riedmatten, P. Goldner, A. Tallaire, L. Morvan, P. Berger, S. Welinski, K. Karrai, L. Rippe, S. Kröll, and A. Walther, "Roadmap for rare-earth quantum computing," arXiv:2103.15743 (2021).
23. S. Hastings-Simon, M. Staudt, M. Afzelius, P. Baldi, D. Jaccard, W. Tittel, and N. Gisin, "Controlled Stark shifts in Er^{3+} -doped crystalline and amorphous waveguides for quantum state storage," *Opt. Commun.* **266**, 716–719 (2006).
24. R. S. Weis and T. K. Gaylord, "Lithium niobate: summary of physical properties and crystal structure," *Appl. Phys.* **37**, 191–203 (1985).
25. A. Guarino, G. Poberaj, D. Rezzonico, R. Degl'Innocenti, and P. Günter, "Electro-optically tunable microring resonators in lithium niobate," *Nat. Photonics* **1**, 407–410 (2007).
26. O. Alibart, V. D'Auria, M. De Micheli, F. Doutre, F. Kaiser, L. Labonté, T. Lunghi, É. Picholle, and S. Tanzilli, "Quantum photonics at telecom wavelengths based on lithium niobate waveguides," *J. Opt.* **18**, 104001 (2016).
27. M. Li, J. I. Ling, Y. He, U. Javid, S. Xue, and Q. Lin, "Lithium niobate photonic-crystal electro-optic modulator," *Nat. Commun.* **11**, 4123 (2020).
28. N. Curtz, R. Thew, C. Simon, N. Gisin, and H. Zbinden, "Coherent frequency-down-conversion interface for quantum repeaters," *Opt. Express* **18**, 22099–22104 (2010).
29. N. Sinclair, E. Saglamyurek, H. Mallahzadeh, J. Slater, M. George, R. Ricken, M. Hedges, D. Oblak, C. Simon, W. Sohler, and W. Tittel, "Spectral multiplexing for scalable quantum photonics using an atomic frequency comb quantum memory and feed-forward control," *Phys. Rev. Lett.* **113**, 053603 (2014).
30. J. Lin, F. Bo, Y. Cheng, and J. Xu, "Advances in on-chip photonic devices based on lithium niobate on insulator," *Photon. Res.* **8**, 1910–1936 (2020).
31. A. Boes, B. Corcoran, L. Chang, J. Bowers, and A. Mitchell, "Status and potential of lithium niobate on insulator (LNOI) for photonic integrated circuits," *Laser Photon. Rev.* **12**, 1700256 (2018).
32. M. Zhang, B. Buscaino, C. Wang, A. Shams-Ansari, C. Reimer, R. Zhu, J. Kahn, and M. Lončar, "Broadband electro-optic frequency comb generation in a lithium niobate microring resonator," *Nature* **568**, 373–377 (2019).
33. C. Wang, M. Zhang, X. Chen, M. Bertrand, A. Shams-Ansari, S. Chandrasekhar, P. Winzer, and M. Lončar, "Integrated lithium niobate electro-optic modulators operating at CMOS-compatible voltages," *Nature* **562**, 101–104 (2018).
34. M. Zhang, C. Wang, R. Cheng, A. Shams-Ansari, and M. Lončar, "Monolithic ultra-high-Q lithium niobate microring resonator," *Optica* **4**, 1536–1537 (2017).
35. Z. Wang, Z. Fang, Z. Liu, W. Chu, Y. Zhou, J. Zhang, R. Wu, M. Wang, T. Lu, and Y. Cheng, "On-chip tunable microdisk laser fabricated on Er^{3+} -doped lithium niobate on insulator," *Opt. Lett.* **46**, 380–383 (2021).
36. L. Yang, S. Wang, M. Shen, Y. Xu, J. Xie, and H. Tang, "Photonic integration of $\text{Er}^{3+}:\text{Y}_2\text{SiO}_5$ with thin-film lithium niobate by flip chip bonding," *Opt. Express* **29**, 15497–15504 (2021).
37. D. Pak, H. An, A. Nandi, X. Jiang, Y. Xuan, and M. Hosseini, "Ytterbium-implanted photonic resonators based on thin film lithium niobate," *J. Appl. Phys.* **128**, 084302 (2020).
38. S. Dutta, E. Goldschmidt, S. Barik, U. Saha, and E. Waks, "Integrated photonic platform for rare-earth ions in thin film lithium niobate," *Nano Lett.* **20**, 741–747 (2020).
39. Z. Kis, G. Mandula, K. Lengyel, I. Hajdara, L. Kovacs, and M. Imlau, "Homogeneous linewidth measurements of Yb^{3+} ions in congruent and stoichiometric lithium niobate crystals," *Opt. Mater.* **37**, 845–853 (2014).
40. S. Welinski, A. Ferrier, M. Afzelius, and P. Goldner, "High-resolution optical spectroscopy and magnetic properties of Yb^{3+} in Y_2SiO_5 ," *Phys. Rev. B* **94**, 155116 (2016).
41. J. Kindem, J. Bartholomew, P. Woodburn, T. Zhong, I. Craiciu, R. Cone, C. Thiel, and A. Faraon, "Characterization of $^{171}\text{Yb}^{3+}:\text{YVO}_4$ for photonic quantum technologies," *Phys. Rev. B* **98**, 024404 (2018).
42. J. Zhu, S. Ozdemir, Y. Xiao, L. Li, L. He, D. Chen, and L. Yang, "On-chip single nanoparticle detection and sizing by mode splitting in an ultrahigh-Q microresonator," *Nat. Photonics* **4**, 46–49 (2010).
43. M. Orrit and J. Bernard, "Single pentacene molecules detected by fluorescence excitation in a p-terphenyl crystal," *Phys. Rev. Lett.* **65**, 2716 (1990).
44. T. Utikal, E. Eichhammer, L. Petersen, A. Renn, S. Götzinger, and V. Sandoghdar, "Spectroscopic detection and state preparation of a single praseodymium ion in a crystal," *Nat. Commun.* **5**, 3627 (2014).
45. I. Nakamura, T. Yoshihiro, H. Inagawa, S. Fujiyoshi, and M. Matsushita, "Spectroscopy of single Pr^{3+} ion in LaF_3 crystal at 1.5 K," *Sci. Rep.* **4**, 7364 (2014).
46. P. Stevenson, C. M. Phenicie, I. Gray, S. P. Horvath, S. Welinski, A. M. Ferrenti, A. Ferrier, P. Goldner, S. Das, R. Ramesh, R. J. Cava, N. P. de Leon, and J. D. Thompson, "Erbium-implanted materials for quantum communication applications," arXiv:2110.04876 (2021).